RSC Advances

PAPER

View Article Online
View Journal | View Issue

Cite this: *RSC Adv.*, 2019, **9**, 25776

How intramolecular coordination bonding (ICB) controls the homolysis of the C–ON bond in alkoxyamines†

Gérard Audran,[a] Elena Bagryanskaya,[bc] Irina Bagryanskaya,[bc] Mariya Edeleva,[*bc] Jean-Patrick Joly,[a] Sylvain R. A. Marque,[*ab] Anna Iurchenkova,[c] Polina Kaletina,[bc] Sergey Cherkasov,[bc] Tung To Hai,[a] Evgeny Tretyakov[bc] and Svetlana Zhivetyeva[b]

Because the C–ON bond homolysis rate constant k_d is an essential parameter of alkoxyamine reactivity, it is especially important to tune k_d without a major alteration of the structure of the molecule. Recently, several approaches have become known, *e.g.*, protonation of functional groups and formation of metal complexes. In this paper, coordination reactions of $[Zn(hfac)_2(H_2O)_2]$ with a series of new SG1-based alkoxyamines affording complexes with different structures are presented. The k_d values of the complexed forms of the alkoxyamines were compared to those of free and protonated ones to reveal the contribution of the electron-withdrawing property and structure stabilization. Together with previously published data, this work provides clues to the design of alkoxyamines that can be effectively activated upon coordination with metal ions. Furthermore, our results provide insight into the mechanism underlying the influence of complexation on the reactivity of alkoxyamines. This led us to describe different types of coordination: intramolecular in nitroxyl fragment, intramolecular in alkyl fragment, intramolecular between alkyl and nitroxyl fragment, and intermolecular one. All of them exhibit different trends which are dramatically altered by changes in conformation.

Received 12th July 2019
Accepted 2nd August 2019

DOI: 10.1039/c9ra05334d

rsc.li/rsc-advances

1 Introduction

Alkoxyamines are compounds that find a wide variety of applications ranging from valuable synthons to initiators of nitroxide-mediated polymerization (NMP)[1] as well as theranostic agents.[2] The rate constant of C–ON bond homolysis k_d is important for these applications.[3] Recently, several methods for tuning k_d without alteration of alkoxyamine structure have become known, *e.g.*, protonation of functional groups[4–6] and formation of complexes with metal ions Zn^{2+},[7] Cu^{2+},[8] or Tb^{3+}.[9] Indeed, complexation is a valuable approach to influence the reactivity of alkoxyamines because it paves the way to metal–polymer complexes and to the tuning of the reactivity of theranostic agents upon reaction with metal-containing proteins *in vivo*.[10,11] Furthermore, formation of complexes of the $Zn(hfac)_2$ electron acceptor matrix with alkoxyamines has a positive effect on NMP because it enhances initiation efficiency.[12]

As we have demonstrated earlier,[7–9] alkoxyamine–metal complexes undergo equilibrium dissociation in solution. One can shift this equilibrium by adding a complexation agent for zinc ions, *e.g.*, pyridine (Py) or bi-pyridine. Considering homolysis rate constants, the values of k_d for complexes differ from the ones for free alkoxyamines because complexation causes a redistribution of C–ON bond polarity owing to the electron-withdrawing effect. Depending on the structure of the complex, researchers can expect either an increase or decrease of k_d. Namely, when coordination involves an alkyl part of an alkoxyamine, k_d can increase and *vice versa*.[13] Shifting of solution equilibrium leads to a gradual change of homolysis rate constant k_d, thus allowing for smart tuning of its value for optimization. Furthermore, the formation of a complex leads to stabilization of alkoxyamine structure. Consequently, we can expect that coordination should have an influence equivalent to both the electronic effect and structure stabilization.

Here we present the synthesis of $Zn(hfac)_2$ complexes with polyfunctional alkoxyamines based on the SG1 nitroxyl radical and its derivatives (Chart 1). We measured homolysis rate constants k_d to evaluate the influence of the coordination. The effect of coordination was compared to that of protonation, intramolecular hydrogen bonds (IHBs) and previously reported complexes (see Chart 2). Together with previously published data, the present work gives some clues to the design of alkoxyamines that can be effectively activated upon coordination with metal ions. Furthermore, our findings provide insight into the mechanism underlying the influence of complexation on reactivity of alkoxyamines. It led

[a]*Aix Marseille Univ, CNRS, ICR, UMR 7273, Case 551, Avenue Escadrille Normandie-Niemen, 13397 Marseille Cedex 20, France. E-mail: Sylvain.marque@univ-amu.fr*

[b]*N. N. Vorozhtsov Novosibirsk Institute of Organic Chemistry SB RAS, 9 Pr. Lavrentjeva, Novosibirsk 630090, Russia. E-mail: edeleva@nioch.nsc.ru*

[c]*Novosibirsk State University, 2 Pirogova Str., Novosibirsk 630090, Russia*

† Electronic supplementary information (ESI) available. CCDC 1878897–1878900, 1878902, 1904966. For ESI and crystallographic data in CIF or other electronic format see DOI: 10.1039/c9ra05334d

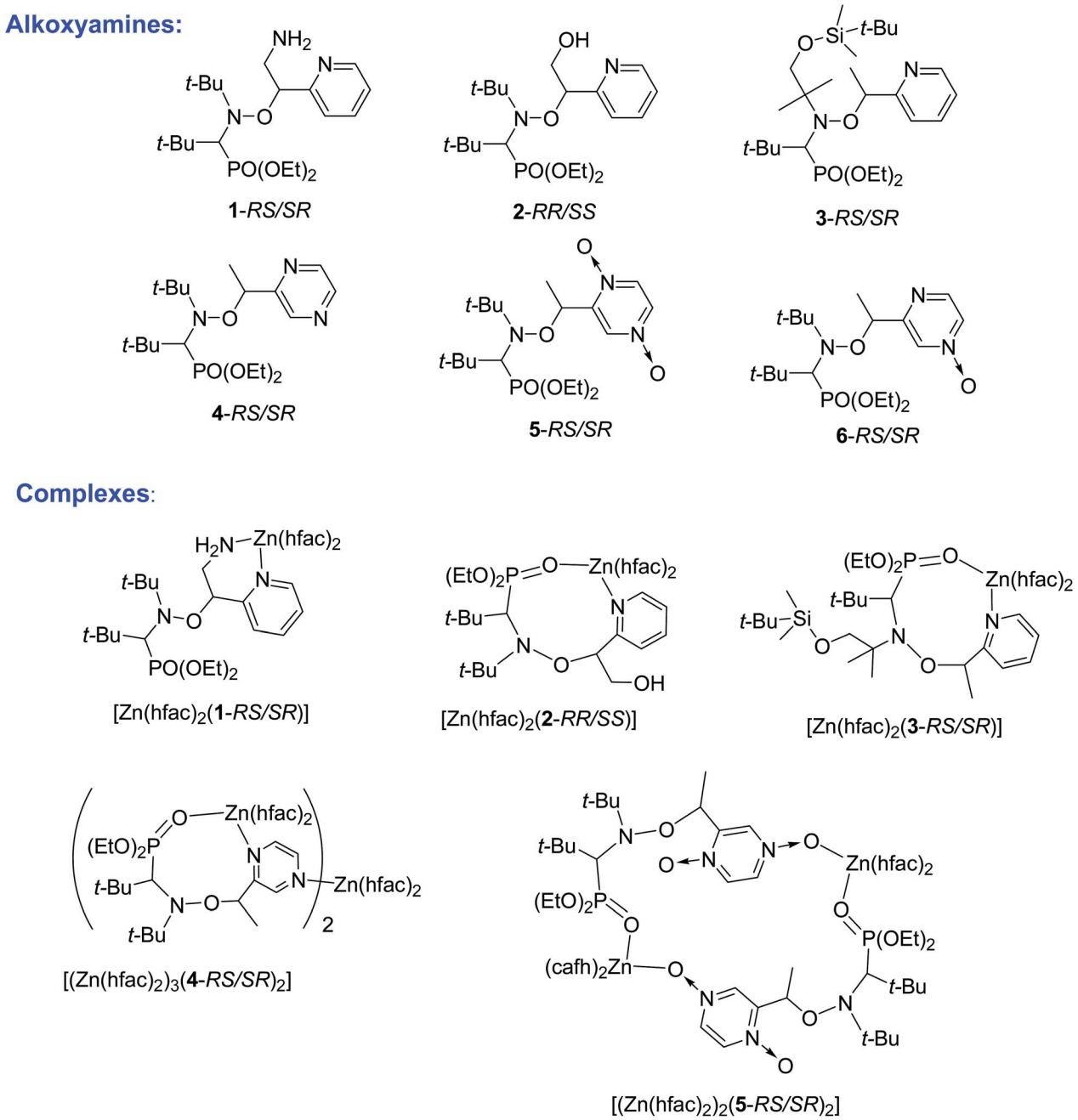

Chart 1 The structures of alkoxyamines and their complexes with $Zn(hfac)_2$ drawn on the basis of XRD data.

us to propose several type of intramolecular coordination bonding (ICB) on the same model as proposed for intramolecular hydrogen-bonding (IHB).[14]

2 Results

Synthesis and structures of complexes

Syntheses of alkoxyamines **1–3** have been described in the literature.[14,15] Alkoxyamines **4–6** are prepared as displayed in Scheme 1, using salen salt procedure and alkene as previously reported.[16] Complexes were prepared according to previously reported procedures.[7,12]

According to our previous observations, the use of the ratio $[Zn(hfac)_2(H_2O)_2]/L^n$ of 1 : 1 as well as the choice of an acetone–heptane mixture as the solvent appear to be suitable for obtaining high-quality crystals of complexes with alkoxyamines. Indeed, under these conditions, the reaction of $[Zn(hfac)_2(H_2O)_2]$ with a racemic mixture of diethyl 1-((2-amino-1-(pyridin-2-yl)ethoxy)(*tert*-butyl)amino)-2,2-dimethylpropylphosphonates (**1**-*RS*/*SR*) formed the cyclic complex $[Zn(hfac)_2(\mathbf{1}\text{-}RS/SR)]$ with a high yield (89%). The complex was formed upon the coordination of alkoxyamine **1**-*RS*/*SR* *via* the two N-atoms of a pyridyl moiety and of the NH_2– group of the alkyl moiety (Fig. 1).

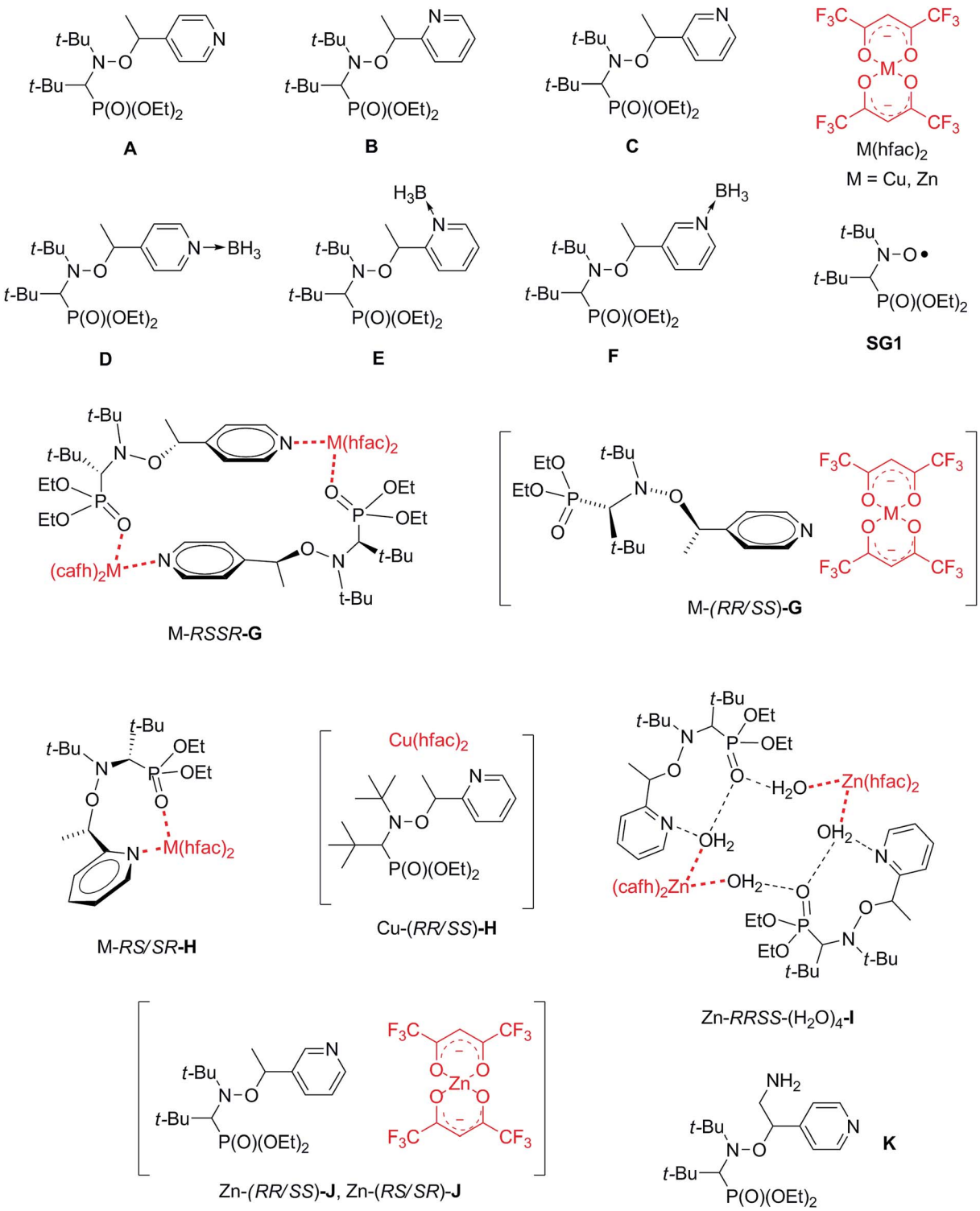

Chart 2 Complexes and alkoxyamine models reported in literature.

According to X-ray analysis, the complex was isolated as a solvate with one molecule of acetone.

Under the same conditions, interaction of $[Zn(hfac)_2(H_2O)_2]$ with a racemic mixture of diethyl 1-(*tert*-butyl(2-hydroxy-1-(pyridin-2-yl)ethoxy)amino)-2,2-dimethylpropylphosphonates (**2**-*RR*/*SS*) or diethyl 1-((1-(*tert*-butyldimethylsilyloxy)-2-methylpropan-2-yl)(1-(pyridin-2-yl)ethoxy)amino)-2,2-dimethylpropylphosphonates (**3**-*RS*/*SR*) afforded cyclic complexes $[Zn(hfac)_2$(**2**-*RR*/*SS*)] and $[Zn(hfac)_2$(**3**-*RS*/*SR*)] containing bidentate alkoxyamines coordinated *via* the N-atom of pyridyl moiety and O-atom of the P=O moiety (Fig. 2). Both complexes were isolated in the form of colorless crystals with high yields (>95%).

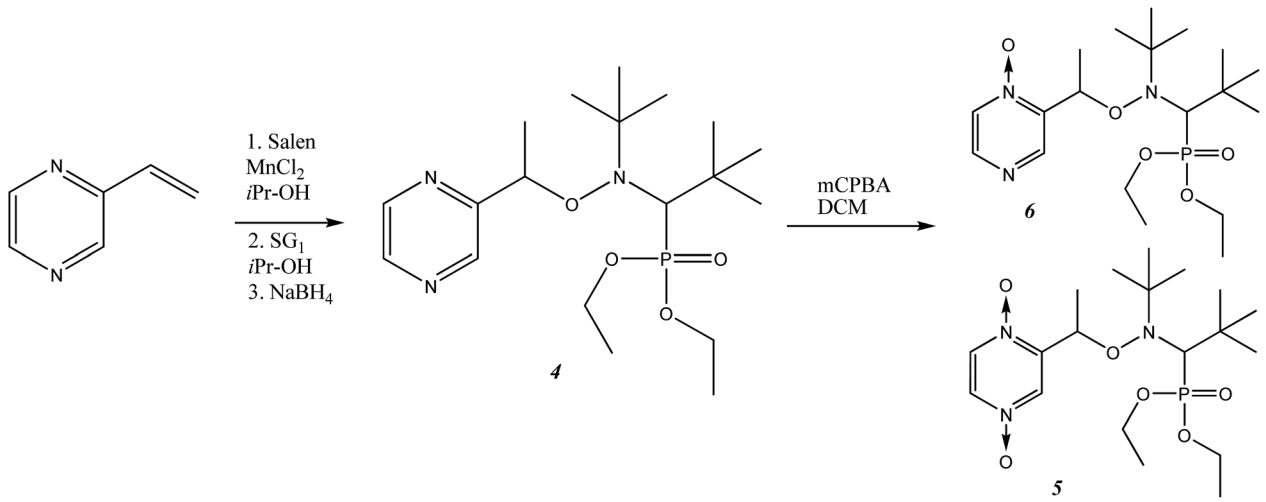

Scheme 1 The synthetic scheme for the preparation of alkoxyamines **4–6**.

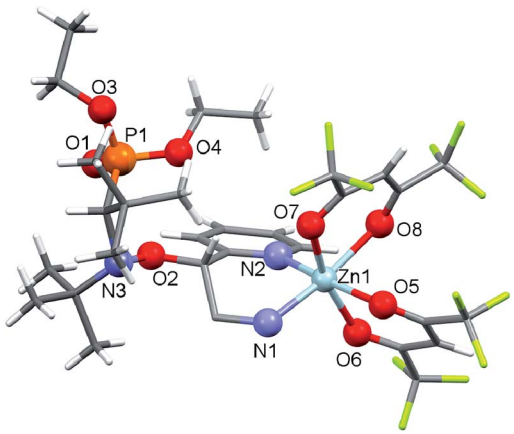

Fig. 1 Molecular structure of [Zn(hfac)$_2$(**1**-*RS*/*SR*)].

Our experiments revealed that the reaction of [Zn(hfac)$_2$(-H$_2$O)$_2$] with the racemic mixture of diethyl 1-(*tert*-butyl(1-(pyrazin-2-yl)ethoxy)amino)-2,2-dimethylpropylphosphonates (**4**-*RS*/*SR*) in the molar ratio 1 : 1 led only to decomposition of initial alkoxyamine **4**-*RS*/*SR*. The use of an appropriate excess of [Zn(hfac)$_2$(H$_2$O)$_2$] in an acetone–heptane mixture resulted in trinuclear complex [(Zn(hfac)$_2$)$_3$(**4**-*RS*/*SR*)$_2$] in a quantitative yield. In the [(Zn(hfac)$_2$)$_3$(**4**-*RS*/*SR*)$_2$] complex, two cyclic parts Zn(hfac)$_2$(**4**-*RS*/*SR*) containing bidentate coordinated ligand **4**-*RS*/*SR* are bound together by the Zn(hfac)$_2$ matrix (Fig. 3).

Under the same conditions, the interaction of [Zn(hfac)$_2$(-H$_2$O)$_2$] with the racemic mixture of the bis-*N*-oxide derivatives (**5**-*RS*/*SR*) in the molar ratio 1 : 1 afforded a centrosymmetric cyclic complex: [(Zn(hfac)$_2$)$_2$(**5**-*RS*/*SR*)$_2$] (Fig. 4). The [(Zn(hfac)$_2$)$_2$(**5**-*RS*/*SR*)$_2$] complex was isolated as pale pink crystals with a high yield (98%).

Thus, the interaction of the Zn(hfac)$_2$ matrix with polyfunctional alkoxyamines **1–5** led to the formation of different complexes as the least soluble species: mononuclear and binuclear cyclic complexes and a trinuclear zinc complex as well. The molecular and crystal structures of all the complexes were solved by monocrystal X-ray diffractometry.

XRD structure of **6** was determined and show all geometrical features already reported for free alkoxyamines based on SG1-nitroxyl fragment and does not deserved more comments.

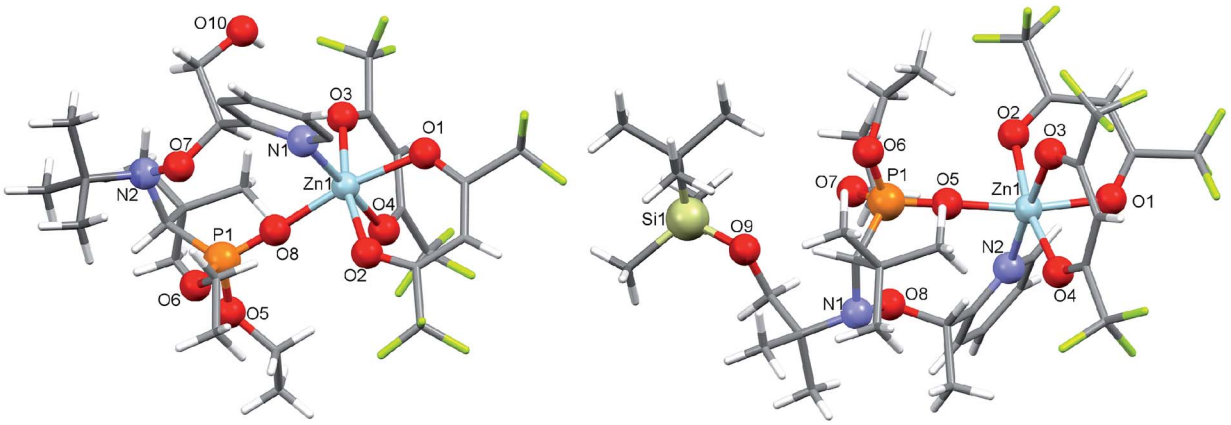

Fig. 2 Molecular structures of [Zn(hfac)$_2$(**2**-*RR*/*SS*)] and [Zn(hfac)$_2$(**3**-*RS*/*SR*)].

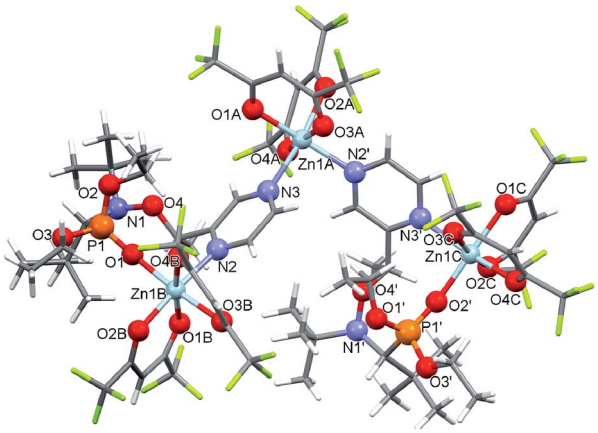

Fig. 3 Molecular structure of $[(Zn(hfac)_2)_3(\mathbf{4}\text{-}RS/SR)_2]$.

NMR analysis

The structure of alkoxyamines and complexes in solution was studied by ^{1}H and ^{31}P NMR analyses. The influence of the complexation was compared to that of protonation. In the solution of $[Zn(hfac)_2(\mathbf{1}\text{-}RS/SR)]$, we observed single resonance at 23.6 ppm in a ^{31}P NMR spectrum (Fig. 6a). The signal was broad, *i.e.*, the width was 40 Hz due to slow chemical exchange between free and complexed forms of the alkoxyamine. Even though X-ray diffraction (XRD) data indicate that the diethylphosphono group is not involved in the complex formation, we observed a significant impact of the complexation on electronic structure of the alkoxyamine P═O group because the ^{31}P resonance of the alkoxyamine ligand differs significantly from that of the free alkoxyamine. Upon gradual addition of pyridine as a competitive ligand, we observed a downfield shift of the signal's chemical shift of the P atom. When 2 equiv. of pyridine were added, the line broadened, meaning an intermediate chemical exchange between different types of complexes present in the solution. Further addition of pyridine resulted in a gradual decrease in the effective concentration of the complex because we observed a constant increase in the ^{31}P chemical shift with a final value of 24.2 ppm. Even in the presence of 100 equiv. of pyridine, we did not observe the complete decomposition of the complex because the value of the chemical shift was different from the free alkoxyamine. It should be noted that protonation of **1** upon addition of 1 equiv. of TFA causes a significant downfield shift of phosphorus signals to 25.0 ppm. In this case, the influence on the δ of the diethylphosphono group is caused by the electron-withdrawing effect of the protonated alkyl moiety of the alkoxyamine.

Complexes $[Zn(hfac)_2(\mathbf{2}\text{-}RR/SS)]$ and $[Zn(hfac)_2(\mathbf{3}\text{-}RS/SR)]$ show similar behavior. The corresponding ^{1}H and ^{31}P NMR spectra are presented as ESI.†

Similarly, the addition of pyridine to the solution of $[(Zn(hfac)_2)_3(\mathbf{4}\text{-}RS/SR)_2]$ results in downshifting of the ^{31}P signal. When 2 to 10 equiv. of pyridine were added, we observed broadening of the signal, implying intermediate chemical exchange. Although no changes are observed in ^{31}P NMR upon addition of 1 equiv. of TFA (Fig. 6b), significant shifts are observed in the aromatic zone upon addition of both 1 and 2 equiv of TFA meaning that the two N-atom of the pyrazyl moiety are successively protonated (Fig. 7) despite pK_a values estimated lower than 1 (see Scheme ESI†).

Differences reported in the aromatic zone and in the zone of nitroxyl fragment in ^{31}P and ^{1}H NMR signals between $[(Zn(hfac)_2)_2(\mathbf{5}\text{-}RS/SR)_2]$ and alkoxyamine **5** denote likely an equilibrium between different isomer of unimeric form as already reported and discussed for Zn-*RSSR*-**G**.[7]

Determination of homolysis rate constants k_d

The results on homolysis rate constant k_d measurements for coordinated, protonated, and pure forms of alkoxyamines are presented in Fig. 8 and in Table 1. For all the species, we observed monoexponential growth of a nitroxide concentration upon heating as displayed in Fig. 8a. In this case, to determine k_d, we fitted the experimental data points to eqn (1):

$$I = I_\infty(1 - e^{-k_d t}) \quad (1)$$

Activation energies were estimated *via* preexponential factor $A_0 = 2.4 \times 10^{14}$ s^{-1}.

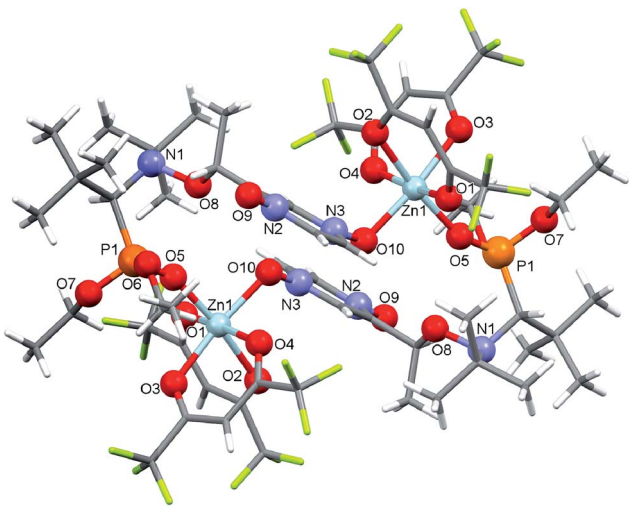

Fig. 4 Molecular structure of cyclic complex $[(Zn(hfac)_2)_2(\mathbf{5}\text{-}RS/SR)_2]$.

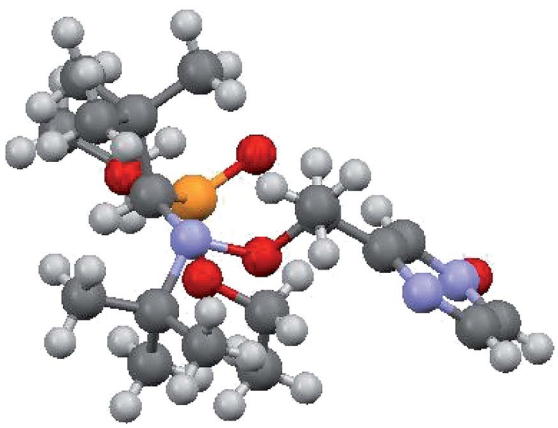

Fig. 5 Molecular structure of **6**.

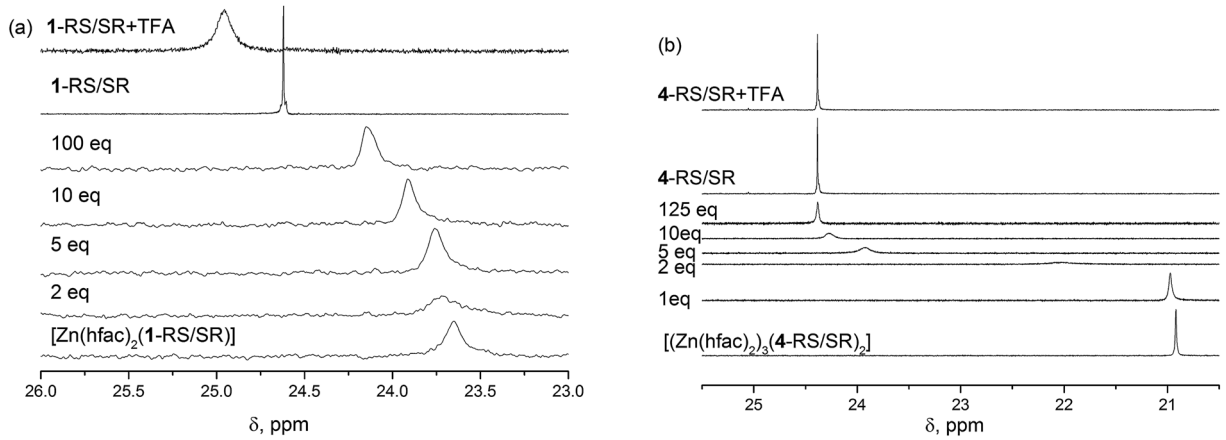

Fig. 6 ^{31}P NMR spectroscopy of [Zn(hfac)$_2$(**1**-*RS*/*SR*)] (a) and of [(Zn(hfac)$_2$)$_3$(**4**-*RS*/*SR*)$_2$] (b) complex in C_6D_6 (0.02 M solution) with different amounts of pyridine as a competitor along with a free alkoxyamine and alkoxyamine with 0.02 M (1 equiv.) of trifluoroacetic acid (TFA).

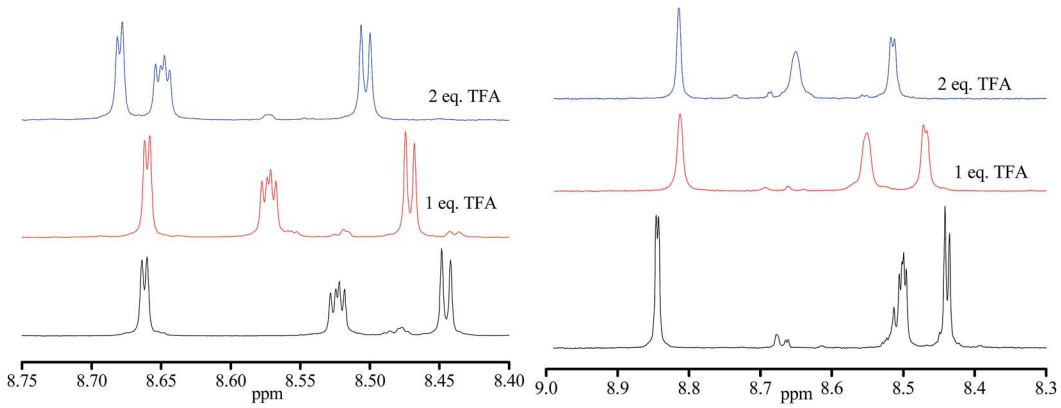

Fig. 7 ^{1}H NMR of aromatic zone in $CDCl_3$ for 0.02 M of *RR*/*SS*-**4** (left) and *RS*/*SR*-**4** (right): non-protonated 4 (bottom), 4 + one equivalent TFA (middle) and 4 + 2 equivalents TFA (top).

We also performed measurement of k_d for [Zn(hfac)$_2$(**1**-*RS*/*SR*)] in the presence of different amounts of pyridine to investigate the behavior of k_d after a gradual decrease in the concentration of the complex. The kinetic curves still had the monoexponential profile, in this case meaning that the equilibrium between the free and complexed forms of an alkoxyamine is reached fast.

3 Discussion

General comments

During the 20 last years, effects ruling the C–ON bond homolysis have been thoroughly investigated.[18,19] General trends have been observed:[18,19] increasing k_d values with increasing

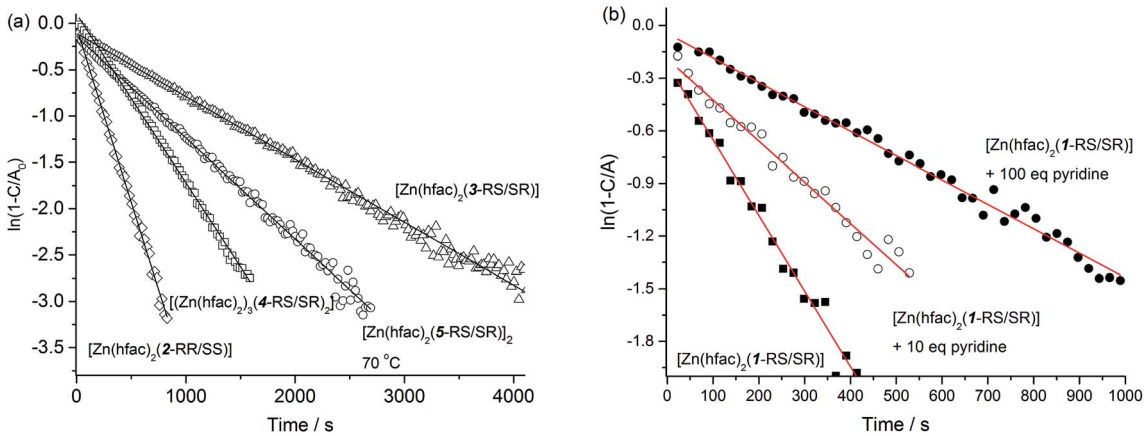

Fig. 8 (a) Experimental kinetics (at 80 °C unless specified otherwise) of homolysis of a complex (in semi-logarithmic coordinates) and their subsequent fit to eqn (1). (b) Experimental kinetics of [Zn(hfac)$_2$(**1**-*RS*/*SR*)] homolysis in the presence of various amount of Py at 80 °C.

Table 1 Homolysis rate constants k_d and activation energies E_a of alkoxyamines and complexes

Compound	Pyridine (equiv.)	T (°C)	k_d[a] (10^{-3} s^{-1})	E_a[b] (kJ mol^{-1})	Ref.
[Zn(hfac)$_2$(**1**-*RS*/*SR*)]	0	80	4.2	113.0	This work
	1	80	3.2	114.0	This work
	10	80	2.4	115.0	This work
	100	80	1.4	116.5	This work
1[j]-*RS*/*SR*	—[c]	100	2.5	121.0	This work
1-*RS*/*SR* + 1 equiv. TFA[k]	—[c]	80	2.6	114.5	This work
[Zn(hfac)$_2$(**2**-*RR*/*SS*)]	0[d]	90	3.8	120.5	This work
2-*RR*/*SS*	—[c]	—	—	121.5	14
2-*RR*/*SS* + 1 equiv. TFA	—[c]	—	—	118.0	15
[Zn(hfac)$_2$(**3**-*RS*/*SR*)]	0	100	6.8	125.0	This work
3-*RS*/*SR*	—[c]	—	—	122.0	14
3-*RS*/*SR* + 1 equiv. TFA	—[c]	—	—	114.0	14
[(Zn(hfac)$_2$)$_3$(**4**-*RS*/*SR*)$_2$]	0	100	1.8	122.0	This work
4[e]-*RS*/*SR*	—[c]	—	—[l]	118.9[l]	This work
4-*RS*/*SR* + 1 equiv. TFA[h]	—[c]	—[m]	—[m]	118.3[m]	This work
4-*RS*/*SR* + 2 equiv. TFA[i]	—[c]	84	1.2	118.4	This work
[(Zn(hfac)$_2$)(**5**-*RS*/*SR*)]$_2$	0	70	1.1	124.0	This work
5[f]-*RS*/*SR*	—[c]	65	1.6	111.1	This work
5-*RS*/*SR* + 1 equiv. TFA	—[c]	70	2.9	111.0	This work
6[g]-*RS*/*SR*	—[c]	70	0.2	118.2	This work

[a] Error 5%. [b] Error at 1 kJ mol^{-1}. [c] Not concerned. [d] At 100 °C, $k_d = 9.7 \times 10^{-3}$ s^{-1}, $E_a = 120.5$ kJ mol^{-1}. [e] For *RR*/*SS* diastereoisomer, $T = 80$ °C, $k_d = 4.5 \times 10^{-4}$ s^{-1}, $E_a = 119.8$ kJ mol^{-1}. [f] For *RR*/*SS* diastereoisomer, $T = 55$ °C, $k_d = 5.5 \times 10^{-4}$ s^{-1}, $E_a = 110.8$ kJ mol^{-1}. [g] For *RR*/*SS* diastereoisomer, $T = 70$ °C, $k_d = 1.5 \times 10^{-4}$ s^{-1}, $E_a = 119.5$ kJ mol^{-1}. [h] For *RR*/*SS* diastereoisomer, $T = 84$ °C, $k_d = 7.8 \times 10^{-4}$ s^{-1}, $E_a = 119.5$ kJ mol^{-1}. [i] For *RR*/*SS* diastereoisomer, $T = 86$ °C, $k_d = 11.5 \times 10^{-4}$ s^{-1}, $E_a = 119.8$ kJ mol^{-1}. [j] For *RS*/*SR*, $T = 80$ °C, $k_d = 2.4 \times 10^{-4}$ s^{-1}, 121.8 kJ mol^{-1}, see ref. 17. [k] For *RS*/*SR*-**1** + 1 equiv. TFA, $T = 61$ °C, $k_d = 7.2 \times 10^{-4}$ s^{-1}, $E_a = 112.1$ kJ mol^{-1}. For *RS*/*SR*-**1** + 2 equiv. of TFA, $T = 61$ °C, $k_d = 7.6 = 10^{-4}$ s^{-1}, $E_a = 111.9$ kJ mol^{-1}, see ref. 17. [l] Averaged value of duplicate experiments: $T = 80$ °C, $k_d = 4.5 \times 10^{-4}$ s^{-1}, $E_a = 119.8$ kJ mol^{-1} and $T = 80$ °C, $k_d = 7.0 \times 10^{-4}$ s^{-1}, $E_a = 118.0$ kJ mol^{-1}. [m] Average value of duplicate experiments: $T = 70$ °C, $k_d = 2.5 \times 10^{-4}$ s^{-1}, $E_a = 118.0$ kJ mol^{-1} and $T = 86$ °C, $k_d = 13.0 \times 10^{-4}$ s^{-1}, $E_a = 118.7$ kJ mol^{-1}.

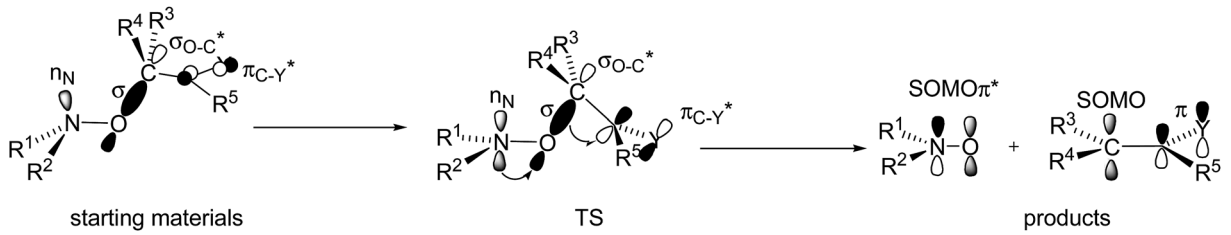

Fig. 9 Orbital interactions and geometries in starting materials (left), at TS (middle), and in products (right).

electronwithdrawing properties and bulkiness of the groups carried by the alkyl fragment,[20,21] with stabilization of the released alkyl and nitroxyl radicals, and, on the other hand, anti-correlated trends[22–24] were reported for the nitroxyl fragments. It led us to define some geometrical requirements and orbital interactions which have to be met at TS (Fig. 9),[18,19,25] that is, dihedral angle θ ⟨OCC=X⟩ close to 90°, dihedral angle ⟨CONlone pair n_N⟩ close to 180°, and flattening at the N-atom of the C–ON moiety, and donation of the lone pair into the antibonding orbital of the C–O bond $n_N \rightarrow \sigma^*_{C-O}$, and then donation of the bonding orbital of the C–O bond into the antibonding orbital of the unsaturated moiety $\sigma_{C-O} \rightarrow \pi^*_{C=X}$.

Based on a large set of data, several empirical or semi-empirical equations accounting for these effects have been proposed.[20,22–24,26,27] However, in most cases, for the chemical activation of the alkoxyamine, these correlations failed to describe and to predict accurate values of k_d although trends are still good. These trends are often modified by changes in conformation caused by large steric repelling interactions or IHB. Recently, we showed that different types of IHB – *intraN*, *interN*, *intraR* and *interR* (Fig. 10) – are possible and modify the basic trends in very different ways.[14] Thus, we proposed to describe the different types of coordination in a similar way (Fig. 10): coordination by bidentate nitroxyl fragment (*intraN*), coordination by bidentate alkyl fragment (*intraR*), coordination by alkyl and nitroxyl fragments (*interF*), and intermolecular coordination bonding, *i.e.*, metal cation coordinated at least by two alkoxyamines. For cases (b–d) and (g) in Fig. 10, the occurrence of IHB or ICB induce the formation of cyclic compounds and, hence, homolysis requires to cleave two bonds: the covalent C–O and the weaker IHB or ICB bond which increases activation energy. However, the occurrence of IHB or ICB implies often changes in conformation which may balance the effect of the second bond, or may strengthened its effect.

IHB and homolysis. As alkoxyamine **K** (Chart 2), which is the regioisomer *para* of **1**, does not display *interR* IHB,‡ it is

‡ Article in preparation.

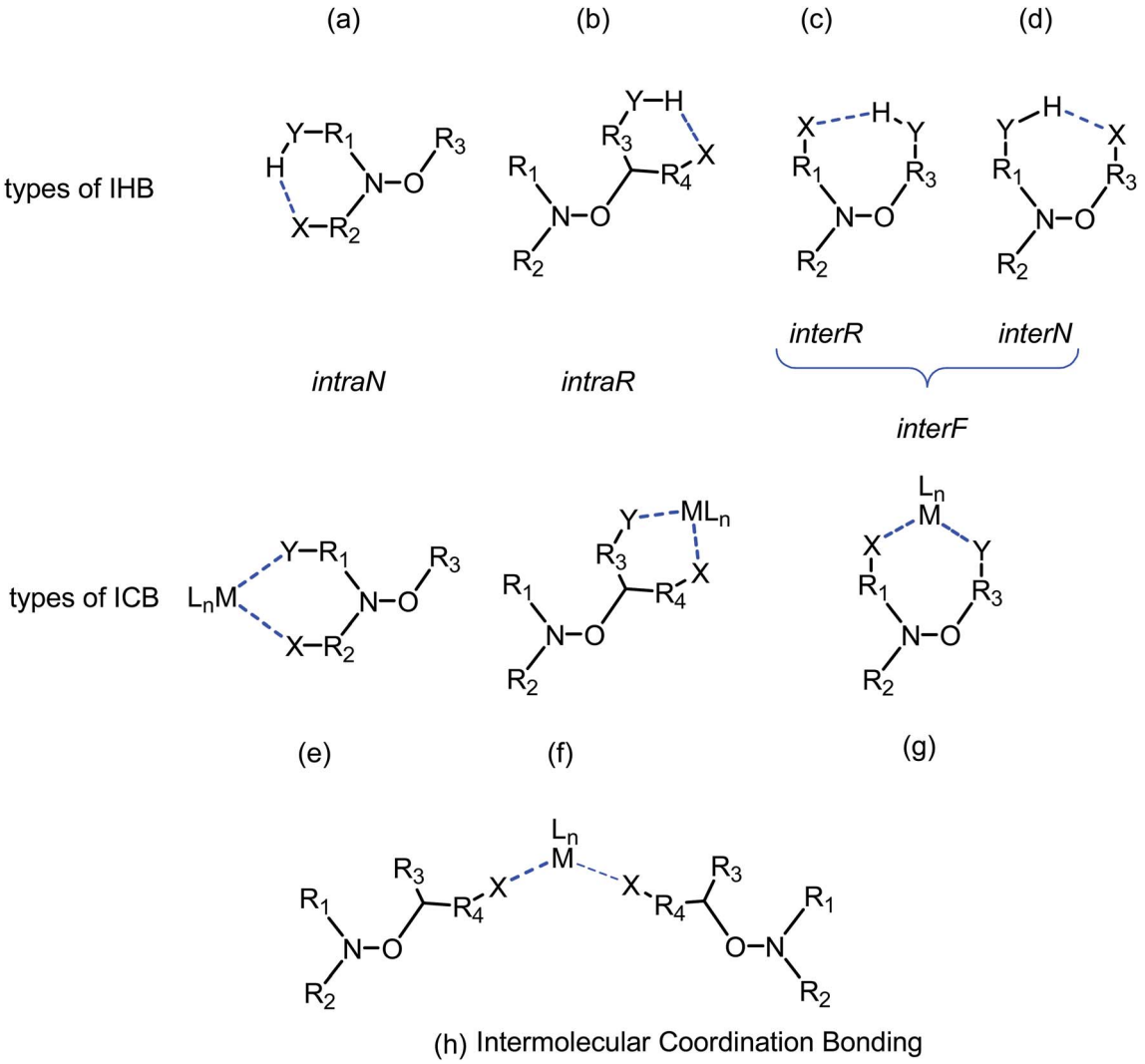

Fig. 10 Various types of IHBs and ICB with metals (dashed blue lines): (a) IHB within the nitroxyl part (*intraN*), (b) IHB within the alkyl part (*intraR*), (c) IHB from an alkyl part to nitroxyl part (*interR*), and (d) IHB from a nitroxyl part to alkyl part (*interN*), (e) ICB within the nitroxyl part (*intraN*), (f) ICB within the alkyl part (*intraR*), (g) ICB between nitroxyl and alkyl parts (*interF*), and intermolecular coordination bonding (h).

assumed that this observation holds for **1**. This assumption is supported by a value of 121 kJ mol^{-1} for **1** which is very close to the value of 124 kJ mol^{-1} for **K**.‡ In general, occurrence of IHB of type *interR* implies an increase of E_a by 10 kJ mol^{-1}.

Kinetics for *RS*/*SR*-**3**, kinetics and IHB for *RR*/*SS*-**2** have been previously reported and do not deserve more comments.[14] Due to the silylation of the hydroxyl group, no IHB occurs in **3**.

Surprisingly, E_a of **4** is 6 kJ mol^{-1} lower than regioisomers *ortho* **B** and *meta* **C**; which are pyridyl models. As stabilization of released radical from **4** is not expected larger than for radical released from **B** and **C**, and as electron withdrawing property of pyrazyl moiety is very close to those of pyridyl moieties, *i.e.*, $\sigma_I = 0.25$ *vs.* $\sigma_I = 0.33$ and $\sigma_I = 0.27$,[28] respectively, this difference in E_a is likely due to change in conformation (*vide infra*).

Alkoxyamines carrying regioisomer *ortho* (**B**); *meta* (**C**), and *para* (**A**) of pyridyl moiety have been oxidized into their corresponding N-oxide. Oxides of **A**[29] and **B**[30] exhibit a decrease of E_a by 10 kJ mol^{-1} according to the non-oxidized regioisomer ($E_a \approx 124$ kJ mol^{-1}) whereas only a decrease by 3 kJ mol^{-1} (ref. 31) is reported for the regioisomer *meta*. The activation is mainly ascribed to the extra stabilization of the released radical in oxidized form (caused by nitroxide mesomeric form) in comparison the non-oxidized alkyl radical.[29–31] Thus, the increase in k_d for the oxidized regio-isomer *meta* is ascribed to a small increase of the polarity. Then, the very close values of E_a for **4** to **6** agree with the non-activating oxidation at the position *meta*. On the other hand, upon oxidation of **4** into **5**, and **5** into **6**, the increase in E_a by 10 kJ mol^{-1} is attributed to effect of extra stabilization of the released alkyl radical as observed for oxidized pyridine *ortho* and *para* derivatives.

Activation by protonation. Protonation of **1**, **2** and **3** has been previously reported and does not deserve more comments.

Thus, to compared the effect of mono-coordination with Zn^{2+} (*vide infra*), 1 equiv. of TFA is added to free alkoxyamine **5**, for which no significant difference is observed, as expected due to the very low basicity of *N*-oxide function. Although pK_a of **4** are very low, mono and diprotonation are observed by ^{1}H NMR (Fig. 7). Nevertheless, no significant effect on k_d (Table 1) is observed for the first protonation likely due to the protonation at the position *meta*.[31] Disappointingly,

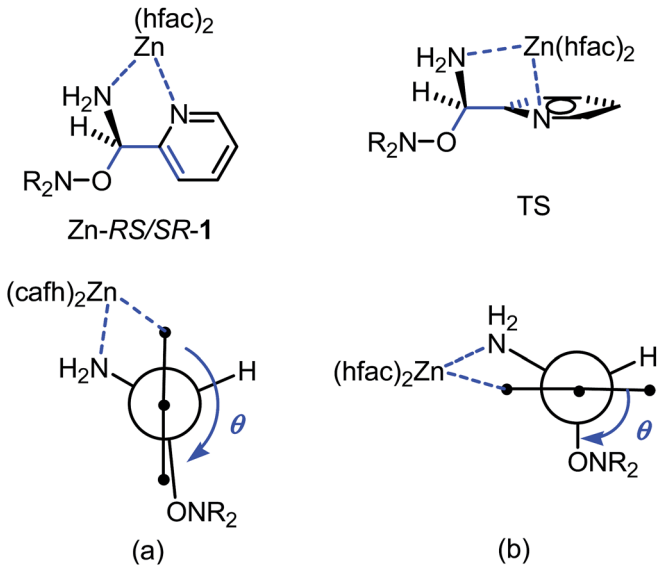

Fig. 11 Newman projections around C_O–C_{aryl} bond in Zn-*RS*/*SR*-**1** in XRD structure (a) and at TS (b). Blue arrow for dihedral angle θ ⟨OCC=C⟩.

no effect (Table 1) is observed for the second protonation as expected for protonation at the position *ortho*.[30] This lack of effect of the protonation might be tentatively ascribed to 3 possibilities: (i) parabolic polar effect;[32] (ii) occurrence of intimate ion pair[33] and its decomposition at high temperature;[29] (iii) conformational effect.§

Coordination effect

IntraR model. At the difference of *RS*/*SR*-**2** for which *interR* IHB is reported,[14] not such an IHB is observed for *RS*/*SR*-**1** meaning that replacing OH group by NH_2 group, both being H-bond donor groups, changes strikingly the structure and the subsequent reactivity. Moreover, the mono protonation of *RS*/*SR*-**1** shows a significant increase in k_d and suggests a strong effect of the coordination of $Zn(hfac)_2$ by **1**. Hence, XRD structure shows a coordination of type *intraR* (Fig. 1 and 10), supported by ^1H and ^{31}P NMR analysis (*vide supra*) in sharp contrast to the *interF* model of coordination observed for Cu-*RS*/*SR*-**B**[8] and Zn-*RS*/*SR*-**C** (*vide infra*).[7] Consequently, a 10-fold increasing in k_d is observed upon the coordination of metal cation Zn(II) by **1** in sharp contrast to *intraR* IHB model *RR*/*SS*-**2** for which no significant differences where observed.[14] Moreover, the change in electronegativity at N-atoms due to *intraR*-type ICB overbalances by 8 kJ mol^{-1} in E_a the entropic cost due to the strongly disfavoured conformation in starting materials accordingly to the geometrical requirements at TS, *i.e.* $\theta = 0°$ *vs.* $\theta = 90°$, respectively (Fig. 10) (Fig. 11).[18,19,25]

InterF ICB. ICB of *interF* type was first reported for Cu-*RS*/*SR*-**H** and Zn-*RS*/*SR*-**H**. For diastereoisomer Cu-*RR*/*SS*-**H**, no crystals were available[8] and for Zn-*RR*/*SS*-**H** dimer was formed involving water molecules bridging alkoxyamine and metal cation Zn^{2+}.[7] Different models were proposed to account for the kinetic results. That is, an equilibrium between Cu-*RS*/*SR*-**H** and Cu(II) coordinated with the alkyl fragment of **B** favouring an activation of the C–ON bond homolysis, *i.e.* a 4-fold increase in k_d was observed,[8] and an equilibrium in favour of Zn-*RS*/*SR*-**H** leading to a small decrease in k_d because of matching between polar effect due to the coordination of the alkyl fragment and the formation of a bridge between alkyl and nitroxyl fragments, *i.e.* a formation of second bond to cleave.[7] For *RR*/*SS* diastereoisomers, coordination of the alkyl fragment is favoured although affording weak activation. The formation of *interF* ICB for both Zn-*RR*/*SS*-**2** and Zn-*RS*/*SR*-**3** denotes that such ICB does not depend straight forwardly on the configuration but more on the conformations allowed by the steric repelling interactions which, in turn, are configuration dependent. As reported for Zn-*RS*/*SR*-**H**, a small 3-fold decrease in k_d is observed for Zn-*RR*/*SS*-**3** and no effect is observed for Zn-*RS*/*SR*-**2**. These differences are likely due to the difference in strength for the coordination bond between the metal cation and the phosphoryl group which is controlled by the

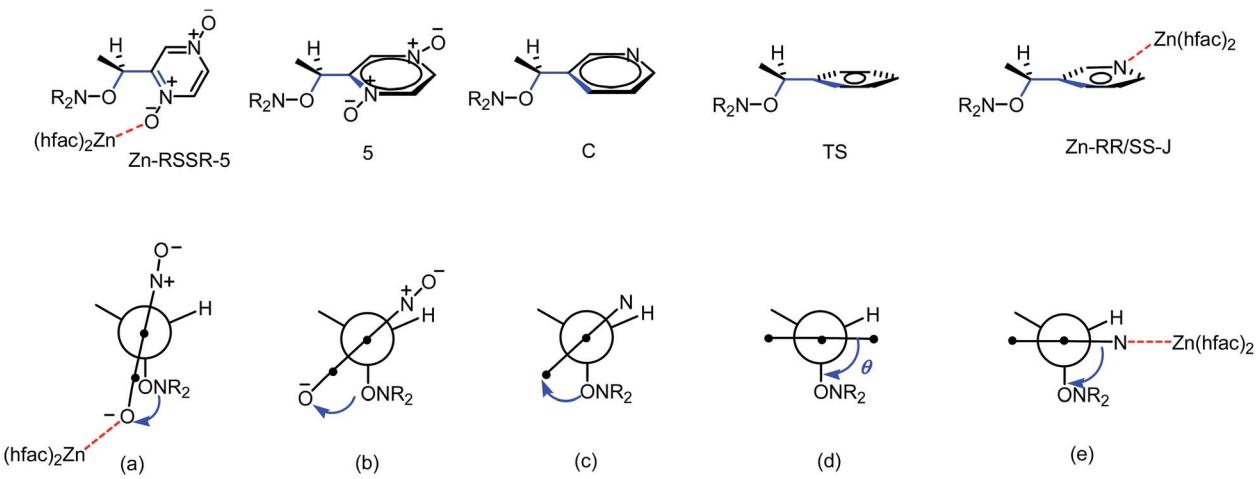

Fig. 12 Newman projections along C_O–C_{aryl} bond for Zn-*RSSR*-**5** (a), 5 (b), C (c), expected TS (d), and Zn-*RR*/*SS*-**J** (e). Blue bonds and blue arrows for dihedral angle θ ⟨OCC_{aryl}⟩ and dotted red lines for coordination bonds.

§ The article considering this effect is in preparation.

Table 2 XRD data on compounds [Zn(hfac)$_2$(**1**-*RS*/*SR*)], [Zn(hfac)$_2$(**2**-*RR*/*SS*)], [Zn(hfac)$_2$(**3**-*RS*/*SR*)], [(Zn(hfac)$_2$)$_3$(**4**-*RS*/*SR*)$_2$], and [(Zn(hfac)$_2$)(**5**-*RS*/*SR*)]$_2$

Compound	[Zn(hfac)$_2$(**1**-*RS*/*SR*)]	[Zn(hfac)$_2$(**2**-*RR*/*SS*)]	[(Zn(hfac)$_2$)(**5**-*RS*/*SR*)]$_2$
Empirical formula	$C_{33}H_{42}F_{12}N_3O_9PZn$	$C_{30}H_{37}F_{12}N_2O_9PZn$	$C_{58}H_{76}F_{24}N_6O_{20}P_2Zn_2$
Formula weight	949.04	893.96	1825.93
Temperature, K	296(2)	296(2)	296(2)
Wavelength, Å	0.71073	0.71073	0.71073
Crystal system	Monoclinic	Monoclinic	Monoclinic
Space group	$P2_1/n$	$P2_1/c$	$P2_1/n$
Unit cell dimensions a, Å	12.4608(7)	13.121(1)	15.7902(6)
b, Å	16.0495(7)	12.1695(9)	11.3758(4)
c, Å	22.7935(11)	25.591(2)	23.2214(11)
α, °	90	90	90
β, °	99.656(2)	98.367(4)	105.424(2)
γ, °	90	90	90
Volume, Å^3	4493.9(4)	4042.7(6)	748.9(1)
Z	4	4	2
Density (calcd), Mg m^{-3}	1.403	1.469	1.508
Abs. coefficient, mm^{-1}	0.680	0.751	0.759
F(000)	1944	1824	1864
Crystal size, mm^3	0.15 × 0.60 × 0.90	0.04 × 0.20 × 0.60	0.15 × 0.25 × 0.40
Θ range for data collection, °	3.1–27.5	3.1–25.0	3.1–26.0
Index ranges	$-16 \le h \le 16$, $-20 \le k \le 20$, $-29 \le l \le 29$	$-15 \le h \le 15$, $-14 \le k \le 14$, $-30 \le l \le 30$	$-19 \le h \le 19$, $-14 \le k \le 14$, $-25 \le l \le 28$
Reflections collected	75 372	56 525	41 980
Independent reflections	10 286 R(int) = 0.048	7134 R(int) = 0.054	1480 R(int) = 0.045
Completeness to θ, %	99.8	99.7	99.8
Data/restraints/parameters	10 286/0/529	7134/0/506	7893/13/594
Goodness-of-fit on F^2	1.07	1.02	1.06
Final R indices $I > 2\sigma(I)$	$R_1 = 0.0529$, w$R_2 = 0.1440$	$R_1 = 0.0702$, w$R_2 = 0.1899$	$R_1 = 0.0453$, w$R_2 = 0.1217$
Final R indices (all data)	$R_1 = 0.0805$, w$R_2 = 0.1840$	$R_1 = 0.1027$, w$R_2 = 0.2488$	$R_1 = 0.0612$, w$R_2 = 0.1366$
Largest diff. peak/hole, e Å^{-3}	0.81/−0.52	0.89/−0.85	0.68/−0.30
Compound	[Zn(hfac)$_3$(**3**-*RS*/*SR*)]	[(Zn(hfac)$_2$)$_3$(**4**-*RS*/*SR*)$_2$]	**6**-*RS*/*SR*
Empirical formula	$C_{36}H_{53}F_{12}N_2O_9PSiZn$	$C_{68}H_{78}F_{36}N_6O_{20}P_2Zn_3$	$C_{19}H_{36}N_3O_5P$
Formula weight	1010.23	2241.41	417.48
Temperature, K	296(2)	200(2)	293
Wavelength, Å	0.71073	0.71073	0.71073
Crystal system	Triclinic	Triclinic	Monoclinic
Space group	$P\bar{1}$	$P\bar{1}$	$C2/c$
Unit cell dimensions a, Å	11.3993(6)	15.4251(6)	16.2198(9)
b, Å	13.6801(8)	17.7197(7)	9.6226(6)
c, Å	16.1856(9)	19.8153(7)	29.4018(18)
α, °	96.668(2)	86.523(2)	90
β, °	94.471(2)	70.3620(10)	93.873(5)
γ, °	100.497(2)	67.3500(10)	90
Volume, Å^3	2452.3(2)	4692.9(3)	4578.5(5)
Z	2	2	8
Density (calcd), Mg m^{-3}	1.368	1.586	1.211
Abs. coefficient, mm^{-1}	0.651	0.931	0.152
F(000)	1044	2264	1808.0
Crystal size, mm^3	0.20 × 0.30 × 0.35	0.03 × 0.15 × 0.40	0.36 × 0.28 × 0.06
Θ range for data collection, °	3.1–27.5	3.0–26.0	5.584–49.426
Index ranges	$-14 \le h \le 14$, $-17 \le k \le 17$, $-21 \le l \le 21$	$-19 \le h \le 19$, $-21 \le k \le 21$, $-24 \le l \le 24$	$-19 \le h \le 19$, $-11 \le k \le 11$, $-22 \le l \le 34$
Reflections collected	75 434	83 455	13 148
Independent reflections	11 207 R(int) = 0.040	18 469 R(int) = 0.034	3887 R(int) = 0.0634
Completeness to θ, %	99.8	99.8	99.8
Data/restraints/parameters	11 207/9/676	18 469/26/1216	3887/0/262
Goodness-of-fit on F^2	1.05	1.04	1.078
Final R indices $I > 2\sigma(I)$	$R_1 = 0.0448$, w$R_2 = 0.1255$	$R_1 = 0.0573$, w$R_2 = 0.1530$	$R_1 = 0.0735$, w$R_2 = 0.2152$
Final R indices (all data)	$R_1 = 0.0686$, w$R_2 = 0.1784$	$R_1 = 0.0740$, w$R_2 = 0.1701$	$R_1 = 0.1172$, w$R_2 = 0.3084$
Largest diff. peak/hole, e Å^{-3}	0.60, −0.61	2.28, −1.10	0.56, −0.67

repelling interactions between alkyl and nitroxyl fragments. *InterF* ICB involving one molecule of water bridging the metal cation Tb^{3+} and the phosphoryl group in **B** was also reported.[9] In solution, such a bridge is expected to collapse and to afford only coordination bond between phosphoryl group and the oxophil metal cation Tb^{3+} affording less than a 3-fold decrease in k_d.[9] It means that the electronwithdrawing effect of the coordination of the phosphoryl group with metal cation is weak, *i.e.*, weak

destabilization of the nitroxyde and small increase in electronegativity at the O-atom of the C–ON moiety.

Intermolecular coordination bonding. Due to the pyrazine moiety in the alkyl fragment, alkoxyamine Zn-*RS*/*SR*-**4** exhibits two sites of coordination: at the *ortho* position providing *interF* coordination between phosphoryl group in the nitroxyl fragment and pyrazine moiety in the alkyl fragment, and at the position *meta* providing, in that case, an intermolecular coordination bonding, *i.e.*, metal cation is coordinated by two alkoxyamines through the *meta* position of the pyrazine moiety.

InterF coordination is expected to decrease k_d as mentioned above and does not deserve more comments. On the other hand, activation at the position *meta* is in general reported as weak, *i.e.*, not more than 4-fold increase in k_d, whatever the mode of activation and the diastereoisomer excepted for Zn-*RR*/*SS*-**J** for which a 30-fold increase in k_d is reported.

As dihedral angle θ $\langle OCC_{aryl} \rangle$ is in the range of 70°,¶ the 3-fold decrease in k_d is then mainly ascribed to the formation of ICB of *interF* type.

Miscellaneous coordination bonding. In this section are gathered all XRD structures which do not display *intraN*, *intraR*, and *interF* ICBs, and intermolecular coordination bonding, that is, dimer as Cu-*RSSR*-**G** and Zn-*RSSR*-**G** (*para* regioisomer **A**), polymer as Cu-*RR*/*SS*-**G** (*para* regioisomer **A**), bridge structure as Zn-*RRSS*-**I** (*ortho* regioisomer **B**), and unknown structures as Zn-*RR*/*SS*-**G** (*para* regioisomer **A**), Cu-*RR*/*SS*-**H** (*ortho* regioisomer **B**), Zn-*RR*/*SS*-**J** and Zn-*RS*/*SR*-**J** (*meta* regioisomer **C**, Chart 2).

Up to now, monocoordination of alkoxyamines has only been investigated with alkyl fragments carrying one pyridyl moiety. It was reported that the influence of coordination depended on the regioisomer, *i.e.*, *para* isomers show an increase of k_d, *meta* isomers show either an increase in k_d (Zn-*RR*/*SS*-**J**) or a decrease in k_d (Zn-*RS*/*SR*-**J**). *Ortho* isomers display, in general, bidentate coordination as discussed above. Interestingly, alkoxyamine Zn-*RSSR*-**5** exhibits a dimer structure very similar to those reported for Zn-*RSSR*-**G** and Cu-*RSSR*-**G**. For both Zn-*RSSR*-**G** and Cu-*RSSR*-**G**, it was assumed that dimer structures were decomposed into unimeric species. We expect that these comments hold also for Zn-*RSSR*-**5** and that the differences in ^{1}H NMR observed between free alkoxyamine *RS*/*SR*-**5** and Zn-*RSSR*-**5** are due to the equilibrium between several conformers as already described.[26] The 50-fold decrease in k_d is the largest de-activation effect of the coordination of alkyl fragment reported up to now and in very sharp contrast with the moderate de-activation effect reported for *interF* and the weak activation effect reported for Zn-*RS*/*SR*-**J** and the strong activation effect for Zn-*RR*/*SS*-**J**. The coordination of the O-atom at the position *meta* should not change the stabilization of the released alkyl radical (same number of mesomer forms than the non-coordinated radical), should slightly increase the polarity of the pyrazinyl ring and should increase the primary steric effect, thus an increase in k_d is expected in very sharp contrast with the 50-fold decrease observed. Thus, this decrease is better ascribed to a change in conformation due to strong repelling interactions between alkyl and nitroxyl fragments. Indeed, the increase in k_d observed for Zn-*RR*/*SS*-**J** for the coordination at the position meta of **C** is ascribed to the change of conformation of the aromatic ring affording a conformation with angle θ close to 90° as required for TS (Fig. 12). Hence, entropic cost is lower in Zn-*RR*/*SS*-**J** than in "*normal*" alkoxyamines, with a value around 60–70° as in **C**, for which to open the angle at the required value has an entropic cost, and a lower entropic cost affords a higher value of k_d. Thus, XDR of **6** (Fig. 5) shows θ = 73° and it is assumed the same value in **5**. Hence, $\theta = 30°$ in Zn-*RSSR*-**5** (Fig. 4) means a high entropic cost to reach the angle required at TS and, consequently, a decrease in k_d from free alkoxyamine **5** to Zn-*RSSR*-**5**.

¶ For alkoxyamines described by multiparameter correlations, values of θ from XRD or DFT calculations are in the range 60–70°.

4 Conclusion

In this paper, we present the synthesis of five new complexes of alkoxyamines (based on the SG1 nitroxide) with $[Zn(hfac)_2(H_2O)_2]$. Depending on the structure of the alkoxyamine ligand, different types of complexes were formed: a 1-to-1 complex with the alkyl part of an alkoxyamine acting like ligand, a 1-to-1 complex with both parts of the alkoxyamine involved in the complexation, a 1-to-2 complex, and ring-type complexes. With these examples, we highlighted several type of ICB as for IHB and we proposed a similar ranking but with strikingly different influence: *intraN* ICB affording a striking decrease in k_d in sharp contrast to *intra*R IHB, *intraR* ICB affording a moderate increase in k_d in contrast to *intra*R IHB for which no effect is observed, *intraF* ICB affording a moderate decrease in k_d as observed for both *interN* and *interR* IHB. Details on *intraN* ICB are reported in a forthcoming article. In contrast to IHB, intermolecular coordination bond is also possible, and the effect of the example reported for Zn-*RS*/*SR*-**4** is mainly controlled by the occurrence of *interF* ICB.

ICB provides a new tool to control the homolysis of the C–ON bond in alkoxyamine in a different way of IHB but applying the same rules. Indeed, the high lability of alkoxyamines may rise several issues in storage, handling and shipping of alkoxyamines as for example **5** has $t_{1/2}$ = 23 hours at 25 °C involving issues whereas Zn-*RSSR*-**5** has $t_{1/2}$ = 182 days making it easier to use.

5 Experimental

Infrared (IR) spectra were recorded on a Bruker Vector 22 spectrometer (KBr). The elemental analyses were performed on a Carlo Erba 1106 CHN elemental analyzer and Euro EA-3000 CHNS elemental analyzers. Solvents and reagents were of reagent quality. Dihydrate of bis(hexafluoroacetylacetonato) zinc(II) was prepared as previously reported.[34]

Preparation of alkoxyamines

Alkoxyamines 4-*RR*/*SS* and 4-*RS*/*SR* (Fig. 8, reaction a). To a stirred solution of salen ligand (84 mg, 0.314 mmol, 0.05 equiv.) in i-PrOH, $MnCl_2$ was added (62 mg, 0.314 mmol, 0.05 equiv.) in an open flask. After 30 min of stirring at room

temperature, a solution of SG1 (1.85 g, 6.281 mmol, 1 equiv.) and 2-vinylpyrazine (1.00 g, 9.422 mmol, 1.5 equiv.) in i-PrOH was added first, then solid $NaBH_4$ (475 mg, 12.560 mmol, 2 equiv.) in small portions. The resulting suspension was stirred at room temperature for 2 h. It was then diluted with EtOAc, and 1 M aq. HCl was carefully added. Solid $NaHCO_3$ was then added until neutralization. The layers were separated, and the organic phase was washed with water and brine and dried over $MgSO_4$. The solvent was evaporated to obtain the crude product as a 1 : 2 mixture of diastereoisomers (^{31}P-NMR ratio). The diastereomers were separated by automatic flash column chromatography (gradient of Et_2O in petroleum ether: 100% EP to 100% Et_2O) to obtain **4**-*RR*/*SS* (0.54 g, 22%) and **4**-*RS*/*SR* (1.41 g, 56%). **4**-*RR*/*SS*; colorless oil; ^{1}H NMR (300 MHz, $CDCl_3$) δ: 8.61 (d, J = 1.5 Hz, 1H), 8.47 (dd, J = 2.6, 1.5 Hz, 1H), 8.39 (d, J = 2.6 Hz, 1H), 5.18 (q, J = 6.8 Hz, 1H), 4.59–4.23 (m, 1H), 4.21–3.78 (m, 3H), 3.31 (d, J^{H-P} = 26.3 Hz, 1H), 1.61 (d, J = 6.8 Hz, 3H), 1.28 (m, 6H), 1.20 (s, 9H), 0.74 (s, 9H). ^{13}C NMR (75 MHz, $CDCl_3$) δ: 158.9 (C ar), 144.6 (CH ar), 143.8 (CH ar), 143.2 (CH ar), 82.8 (CH), 69.8 (d, J = 139.4 Hz, CH), 61.7 (d, J = 6.4 Hz, CH_2), 61.4 (C), 59.1 (d, J = 7.5 Hz, CH_2), 35.6 (d, J = 5.2 Hz, C), 30.4 (d, J = 5.9 Hz, CH_3), 28.4 (CH_3), 21.5 (CH_3), 16.7 (d, J = 5.8 Hz, CH_3), 16.3 (d, J = 6.6 Hz, CH_3). ^{31}P NMR (121 MHz, $CDCl_3$) δ: 25.27. HRMS *m*/*z* (ESI) calcd for $C_{19}H_{37}N_3O_4P$ $[M + H]^+$ 402.2516, found: 402.2514. **4**-*RS*/*SR*; colorless crystal; ^{1}H NMR (300 MHz, $CDCl_3$) δ: 8.77 (d, J = 1.5 Hz, 1H), 8.42 (dd, J = 2.6, 1.5 Hz, 1H), 8.36 (d, J = 2.5 Hz, 1H), 5.30 (q, J = 6.6 Hz, 1H), 4.21–3.78 (m, 2H), 3.66–3.45 (m, 2H), 3.37 (d, J^{H-P} = 26.7 Hz, 1H), 1.55 (d, J = 6.6 Hz, 3H), 1.16 (t, J = 7.1 Hz, 3H), 1.15 (s, 9H), 1.11 (s, 9H), 0.93 (t, J = 7.1 Hz, 3H). ^{13}C NMR (75 MHz, $CDCl_3$) δ: 157.6 (C ar), 144.6 (CH ar), 143.5 (CH ar), 143.2 (CH ar), 77.7 (CH), 69.7 (d, J = 138.9 Hz, CH), 61.5 (C), 61.1 (d, J = 6.9 Hz, CH_2), 59.4 (d, J = 7.5 Hz CH_2), 35.3 (d, J = 4.8 Hz, C), 30.6 (d, J = 6.0 Hz, CH_3), 28.2 (CH_3), 19.7 (CH_3), 16.2 (d, J = 5.8 Hz, CH_3), 16.1 (d, J = 5.8 Hz, CH_3). ^{31}P NMR (121 MHz, $CDCl_3$) δ: 24.64. HRMS *m*/*z* (ESI) calcd for $C_{19}H_{37}N_3O_4P$ $[M + H]^+$ 402.2516, found: 402.2516.

Alkoxyamines 5-*RR*/*SS* and 6-*RR*/*SS* (Fig. 8, reaction b). To a solution of **4**-*RR*/*SS* (0.5 g, 1.24 mmol, 1 equiv.) in dichloromethane (DCM, 25 mL), *m*-CPBA (1.4 g, 6.23 mmol, 5 equiv.) was added, and the mixture was stirred overnight at room temperature under argon. Then, the reaction was quenched with a 10% aqueous solution of sodium sulfite (20 mL) and extracted with DCM (3 × 10 mL). The organic layer was washed with aqueous $NaHCO_3$ sat. and with brine and dried with $MgSO_4$. The solvent was evaporated to obtain a crude product as a mixture of mono-oxidized **6**-*RR*/*SS* and di-oxidized pyrazine **5**-*RR*/*SS*. The mono- and di-oxidized pyrazine were separated by automatic flash column chromatography (gradient of MeOH in DCM, 100% DCM to 85% DCM) to prepare **6**-*RR*/*SS* (263 mg, 51%) and **5**-*RR*/*SS* (91 mg, 17%). **6**-*RR*/*SS*; pale yellow oil; ^{1}H NMR (300 MHz, $CDCl_3$) δ: 8.37 (d, J = 4.0 Hz, 1H), 8.22–8.05 (m, 1H), 7.97 (dd, J = 4.0, 1.5 Hz, 1H), 5.09 (q, J = 6.7 Hz, 1H), 4.43–4.21 (m, 1H), 4.16–3.90 (m, 3H), 3.33 (d, J^{H-P} = 26.4 Hz, 1H), 1.60 (d, J = 6.8 Hz, 3H), 1.30 (m, 6H), 1.20 (s, 9H), 0.87 (s, 9H). ^{13}C NMR (75 MHz, $CDCl_3$) δ: 163.5 (C ar), 146.7 (CH ar), 132.9 (CH ar), 132.4 (CH ar), 82.6 (CH), 69.7 (d, J = 139.7 Hz, CH), 61.8 (d, J = 6.6 Hz, CH_2), 61.7 (C), 59.5 (d, J = 7.5 Hz, CH_2), 35.6 (d, J = 5.0 Hz, C), 30.4 (d, J = 6.0 Hz, CH_3), 28.4 (CH_3), 21.4 (CH_3), 16.7 (d, J = 5.7 Hz, CH_3), 16.3 (d, J = 6.7 Hz, CH_3). ^{31}P NMR (121 MHz, $CDCl_3$) δ: 25.01. HRMS *m*/*z* (ESI) calcd for $C_{19}H_{37}N_3O_5P$ $[M + H]^+$ 418.2465, found: 418.2465. **5**-*RR*/*SS*; yellow oil; ^{1}H NMR (400 MHz, $CDCl_3$) δ: 8.24 (m, 1H), 7.99 (d, J = 4.8 Hz, 1H), 7.92 (m, 1H), 5.61 (q, J = 6.7 Hz, 1H), 4.41–4.21 (m, 1H), 4.17–3.90 (m, 3H), 3.32 (d, J^{H-P} = 26.2 Hz, 1H), 1.66 (d, J = 6.6 Hz, 3H), 1.33 (m, 6H), 1.19 (s, 9H), 1.03 (s, 9H). ^{13}C NMR (75 MHz, $CDCl_3$) δ: 153.2 (C ar), 136.1 (CH ar), 135.1 (CH ar), 134.6 (CH ar), 69.3 (d, J = 139.4 Hz, CH), 62.2 (C), 61.6 (d, J = 6.8 Hz CH_2), 59.9 (d, J = 7.4 Hz, CH_2), 35.7 (d, J = 4.9 Hz, C), 30.0 (d, J = 5.8 Hz, CH_3), 28.2 (CH_3), 20.6 (CH_3), 16.7 (d, J = 5.3 Hz, CH_3), 16.2 (d, J = 6.8 Hz, CH_3). ^{31}P NMR (121 MHz, $CDCl_3$) δ: 24.76. HRMS *m*/*z* (ESI) calcd for $C_{19}H_{37}N_3O_6P$ $[M + H]^+$ 434.2415, found: 434.2414.

Alkoxyamine 5-*RS*/*SR*. Alkoxyamine **5**-*RS*/*SR* was synthesized from **4**-*RS*/*SR* (1.1 g, 2.74 mmol) following the same procedure as for **5**-*RR*/*SS*. Yield 225 mg (19%), yellow crystal; ^{1}H NMR (400 MHz, $CDCl_3$) δ: 8.45 (d, J = 2.4 Hz, 1H), 7.95 (d, J = 5.5 Hz, 1H), 7.89 (m, 1H), 5.48 (q, J = 6.5 Hz, 1H), 4.30–3.75 (m, 4H), 3.40 (d, J^{H-P} = 27.5 Hz, 1H), 1.55 (d, J = 6.5 Hz, 3H), 1.33–1.14 (m, 15H), 1.07 (s, 9H). ^{13}C NMR (75 MHz, $CDCl_3$) δ: 152.4 (C ar), 135.8 (CH ar), 135.1 (CH ar), 134.3 (CH ar), 73.2 (CH), 68.9 (d, J = 138.6 Hz, CH), 62.0 (C), 61.3 (d, J = 7.2 Hz, CH_2), 60.2 (d, J = 7.7 Hz, CH_2), 35.5 (d, J = 4.8 Hz, C), 30.4 (d, J = 5.7 Hz, CH_3), 28.3 (CH_3), 18.1 (CH_3), 16.4 (d, J = 6.1 Hz, CH_3), 16.2 (d, J = 6.7 Hz, CH_3). ^{31}P NMR (121 MHz, $CDCl_3$) δ: 24.55. HRMS *m*/*z* (ESI) calcd for $C_{19}H_{37}N_3O_6P$ $[M + H]^+$ 434.2415, found: 434.2410.

General procedure for preparation of complexes [Zn(hfac)$_2$(1-*RS*/*SR*)] and [Zn(hfac)$_2$(2-*RR*/*SS*)]. A solution of $[Zn(hfac)_2(H_2O)_2]$ (0.025 g, 0.048 mmol) in a mixture of acetone (0.5 mL) and heptane (0.5 mL) was added dropwise to a solution of alkoxyamine **1** or **2** (0.02 g, 0.048 mmol) in a mixture of acetone (0.5 mL) and heptane (0.5 mL). The reaction mixture was stirred at room temperature for 5 min and kept in a refrigerator at 5 °C for 3 days in an open flat-bottom flask to obtain the corresponding product, which was filtered off and air dried.

[(Zn(hfac)$_2$)$_2$(1-*RS*/*SR*)]·acetone. [(Zn(hfac)$_2$)$_2$(**1**-*RS*/*SR*)]·acetone; yield 0.041 g (89%). Anal. calcd. for $C_{33}H_{46}ZnF_{12}N_3O_9P$: C, 41.59; H, 4.86; N, 4.41; found: C, 41.77; H, 4.89; N, 4.58. IR (neat): 3435 vw, 3311 vw, 3236 w, 3163 w, 2995 w, 2982 w, 2910 vw, 2879 vw, 1714 w, 1660 s, 1651 s, 1606 w, 1578 w, 1552 m, 1527 m, 1504 m, 1485 m, 1443 w, 1396 w, 1367 w, 1350 w, 1255 vs, 1203 vs, 1144 vs, 1097 w, 1053 m, 1026 m, 982 w, 968 w, 951 w, 806 w, 791 m, 775 w, 762 w, 742 vw, 665 m, 642 w, 582 w, 555 vw, 527 w cm^{-1}. Crystal growth: a solution of the complex (0.040 g) in an acetone/heptane mixture (1 : 1; 2 mL) was kept in a refrigerator at 5 °C for 72 h to prepare colorless crystals of the solvate complex.

[Zn(hfac)$_2$(2-*RR*/*SS*)]. [Zn(hfac)$_2$(**2**-*RR*/*SS*)]; yield 0.042 g (97%). Anal. calcd. for $C_{30}H_{39}ZnF_{12}N_2O_9P$: C, 40.21; H, 4.39; N, 3.13; found: C, 40.14; H, 4.18; N, 3.18. IR (neat): 3549 vw, 3458 vw, 2989 w, 2941 w, 2910 w, 2877 vw, 1653 s, 1608 w, 1576 w, 1554 m, 1527 m, 1500 m, 1446 w, 1398 w, 1367 w, 1346 w, 1257 vs, 1201 vs, 1146 vs, 1097 m, 1055 m, 1022 m, 976 w, 795 m, 766 w, 744 w, 667 w, 627 vw, 584 w, 559 w, 525 vw cm^{-1}. Crystal growth: a solution of the complex (0.040 g) in an acetone/

heptane mixture (1 : 2; 2 mL) was kept in a refrigerator at 5 °C for 7 days to obtain colorless crystals suitable for XRD.

Preparation of the [Zn(hfac)$_2$(3-*RS*/*SR*)] complex. A solution of [Zn(hfac)$_2$(H$_2$O)$_2$] (0.019 g, 0.038 mmol) in a mixture of acetone (0.5 mL) and heptane (0.5 mL) was added dropwise to a solution of an alkoxyamine (0.02 g, 0.038 mmol) in a mixture of acetone (0.5 mL) and heptane (0.5 mL). The reaction mixture was stirred at room temperature for 30 min and kept in a refrigerator at 5 °C for 5 days in an open flat-bottom flask to prepare the title product, which was then separated and air dried. Yield 0.037 g (97%). Anal. calc. for $C_{36}H_{53}ZnF_{12}N_2O_9PSi$: C, 42.80; H, 5.29; N, 2.77; found: C, 43.05; H, 5.28; N, 2.72. IR (neat): 3433 vw, 2999 w, 2982 w, 2956 w, 2935 w, 2862 w, 1660 s, 1653 s, 1608 w, 1574 w, 1552 m, 1527 m, 1504 m, 1444 w, 1396 w, 1369 w, 1338 w, 1255 vs, 1223 s, 1203 vs, 1147 vs, 1088 m, 1059 m, 1026 m, 972 w, 897 vw, 849 m, 808 w, 793 m, 764 w, 665 m, 623 vw, 582 w, 557 vw, 525 vw, 471 vw cm^{-1}. Crystal growth: a solution of the complex (0.040 g) in an acetone/heptane mixture (1 : 1; 3 mL) was kept in a refrigerator at 5 °C for 5 days. Colorless crystals were separated and air dried.

Preparation of the [(Zn(hfac)$_2$)$_3$(4-*RS*/*SR*)$_2$] complex. A solution of [Zn(hfac)$_2$(H$_2$O)$_2$] (0.039 g, 0.075 mmol) in a mixture of acetone (0.5 mL) and heptane (1.0 mL) was added dropwise to a solution of an alkoxyamine (0.020 g, 0.050 mmol) in a mixture of acetone (0.5 mL) and heptane (1.0 mL). The reaction mixture was stirred at room temperature for 30 min and kept in a refrigerator at 5 °C for 7 days in an open flat-bottom flask to obtain the title complex, which was then separated and air dried. Yield 0.056 g (100%). Anal. calc. for $C_{68}H_{78}Zn_3F_{36}N_6O_{20}P_2$: C, 36.44; H, 3.51; N, 3.75; found: C, 36.47; H, 3.40; N, 3.78. IR (neat): 3433 w, 3140 vw, 2997 w, 2985 w, 2945 vw, 2879 vw, 1730 vw, 1659 s, 1649 s, 1616 w, 1597 w, 1556 m, 1531 m, 1498 m, 1483 m, 1414 w, 1398 w, 1371 w, 1346 w, 1259 vs, 1203 s, 1147 vs, 1099 m, 1076 w, 1059 w, 1041 w, 1024 w, 978 w, 951 vw, 856 vw, 796 w, 766 vw, 742 vw, 667 m, 619 vw, 584 w, 527 vw, 442 vw cm^{-1}. Crystals for XRD were grown by slow evaporation of the acetone/heptane solution (1 : 2) at 5 °C.

Preparation of the [(Zn(hfac)$_2$)$_2$(5-*RS*/*SR*)$_2$] complex. A solution of [Zn(hfac)$_2$(H$_2$O)$_2$] (0.024 g, 0.046 mmol) in a mixture of acetone (0.5 mL) and heptane (1.0 mL) was added dropwise to a solution of an alkoxyamine (0.020 g, 0.046 mmol) in a mixture of acetone (0.5 mL) and heptane (1.0 mL). The reaction mixture was stirred at room temperature for 30 min and kept in a refrigerator at 5 °C for 10 days in an open flat-bottom flask to prepare the corresponding product, which was then separated, air dried, and crystallized from a mixture of CH_2Cl_2 and heptane (1 : 3) to obtain 0.041 g of the title compound (98%). Anal. calc. for $C_{58}H_{76}Zn_2F_{24}N_6O_{20}P_2$: C, 38.15; H, 4.20; N, 4.60; found: C, 38.32; H, 4.10; N, 4.50. IR (neat): 3423 vw, 3144 vw, 3124 vw, 3101 vw, 3001 w, 2983 w, 2937 w, 2883 vw, 1659 s, 1649 s, 1616 w, 1591 w, 1554 m, 1527 m, 1495 s, 1421 s, 1398 w, 1371 w, 1344 w, 1309 w, 1282 m, 1257 vs, 1201 vs, 1149 vs, 1093 m, 1053 m, 1026 m, 980 w, 968 w, 935 vw, 881 vw, 845 w, 833 w, 823 w, 795 m, 775 w, 766 w, 752 w, 742 w, 665 m, 621 w, 582 m, 534 w, 503 vw, 415 vw cm^{-1}. Crystal growth: a solution of the complex in a CH_2Cl_2/heptane mixture (1 : 3; 4 mL) was kept in a refrigerator at 5 °C for 16 days. Pale pink crystals were separated and air dried.

XRD analysis

X-ray crystallographic analyses of the crystals were carried out on a Bruker Kappa Apex II CCD diffractometer using φ,ω-scans of narrow (0.5°) frames with Mo Kα radiation (λ = 0.71073 Å) and a graphite monochromator. The structure was solved by direct methods and refined *via* a full-matrix least-squares method using the SHELX-97 software suite.[35] The positions of hydrogen atoms were calculated *via* the riding model. Absorption corrections were applied by the empirical multiscan method in the SADABS software.[36] The structure of [(Zn(hfac)$_2$)$_2$(5-*RS*/*SR*)$_2$] is formed by crystallographically independent 1/2 part of the molecule. In all structures, the same part of CF_3– groups is disordered by two positions. Notably, such disordering of CF_3– groups is quite typical. Compounds [Zn(hfac)$_2$(1-*RS*/*SR*)], [Zn(hfac)$_2$(2-*RR*/*SS*)], and [(Zn(hfac)$_2$)$_2$(5-*RS*/*SR*)$_2$] crystallized in monoclinic space groups P2$_1$/*n*, *P*2$_1$/*c*, P2$_1$/*n*, and *Cc* accordingly, whereas [Zn(hfac)$_2$(3-*RS*/*SR*)] and [(Zn(hfac)$_2$)$_3$(4-*RS*/*SR*)$_2$] crystallized in triclinic $P\bar{1}$. Their crystallographic data are listed in Table 2. Molecular structures of [Zn(hfac)$_2$(1-*RS*/*SR*)], [Zn(hfac)$_2$(2-*RR*/*SS*)], [Zn(hfac)$_2$(3-*RS*/*SR*)], [(Zn(hfac)$_2$)$_3$(4-*RS*/*SR*)$_2$], and [(Zn(hfac)$_2$)$_2$(5-*RS*/*SR*)$_2$] are shown in Fig. 1–5 with 30% thermal ellipsoid. The obtained crystal structures were analyzed for short contacts between nonbonded atoms in PLATON[37,38] and MERCURY software.[39] CCDC 1878897 ([Zn(hfac)$_2$(1-*RS*/*SR*)]), 1878898 ([Zn(hfac)$_2$(2-*RR*/*SS*)]), 1878899 ([Zn(hfac)$_2$(3-*RS*/*SR*)]), 1878900 ([(Zn(hfac)$_2$)$_3$(4-*RS*/*SR*)$_2$]), 1878902 ([(Zn(hfac)$_2$)$_2$(5-*RS*/*SR*)$_2$]), 1904966 **6**-*RS*/*SR* contain the supplementary crystallographic data for this paper.

^{31}P NMR analyses

^{31}P NMR spectra were acquired for 0.01 M solutions of compounds [Zn(hfac)$_2$(1-*RS*/*SR*)] (with respect to phosphorus) in deuterated benzene on a conventional NMR spectrometer operating at the resonance frequency of protons 500 MHz. For ^{31}P spectroscopy, the signal of H_3PO_4 served as an external reference. A total of 1024 scans were collected to achieve a good signal-to-noise ratio.

EPR-based determination of homolysis rate constants k_d

EPR experiments were performed on a SpinScan EPR machine (Adani). The values of k_d were measured by recording ESR spectra upon heating of 10^{-4} M toluene solutions of complexes and alkoxyamines in the presence of 3 equiv. of 2,2,6,6-tetramethylpiperidine-*N*-oxyl radical (TEMPO) as an alkyl radical scavenger. To generate protonated forms, TFA was used. The solutions were degassed by three cycles of freeze–pump–thaw and sealed in an argon atmosphere prior to measurements to ensure narrow ESR signals of nitroxide SG1 generated in the course of heating. Profiles of the relative concentration were obtained by integration of the low-field EPR line of SG1. Depending on the form of kinetics, experimental data points were fitted to monoexponential eqn (1) (see main text).

Conflicts of interest

Authors declare no conflicts of interest.

Acknowledgements

The authors would like to acknowledge the Ministry of Education and Science of the Russian Federation (state contract No. 2017-220-06-7355) and RSF (grant No. 17-73-10101) for financial support. The authors are also grateful to the Multi-Access Chemical Research Center SB RAS for spectral and analytical measurements. SRAM, GA, THT and JPJ thank Aix-Marseille University and CNRS for support, and ANR for funding (ANR ANR-14-CE16-0023-01). The English language was corrected and certified by http://shevchuk-editing.com.

References

1 D. Gigmes, *Nitroxide mediated polymerization: from fundamentals to applications in materials science*, Royal Society of Chemistry, 2016.
2 G. Audran, P. Brémond, J.-M. Franconi, S. R. Marque, P. Massot, P. Mellet, E. Parzy and E. Thiaudière, *Org. Biomol. Chem.*, 2014, **12**, 719–723.
3 F. Chauvin, P.-E. Dufils, D. Gigmes, Y. Guillaneuf, S. R. Marque, P. Tordo and D. Bertin, *Macromolecules*, 2006, **39**, 5238–5250.
4 P. Brémond and S. R. Marque, *Chem. Commun.*, 2011, **47**, 4291–4293.
5 M. V. Edeleva, I. A. Kirilyuk, I. F. Zhurko, D. A. Parkhomenko, Y. P. Tsentalovich and E. G. Bagryanskaya, *J. Org. Chem.*, 2011, **76**, 5558–5573.
6 E. Bagryanskaya, P. Brémond, M. Edeleva, S. R. Marque, D. Parkhomenko, V. Roubaud and D. Siri, *Macromol. Rapid Commun.*, 2012, **33**, 152–157.
7 G. Audran, E. Bagryanskaya, I. Bagryanskaya, M. Edeleva, S. R. Marque, D. Parkhomenko, E. Tretyakov and S. Zhivetyeva, *ChemistrySelect*, 2017, **2**, 3584–3593.
8 G. Audran, E. Bagryanskaya, I. Bagryanskaya, P. Brémond, M. Edeleva, S. R. Marque, D. Parkhomenko, E. Tretyakov and S. Zhivetyeva, *Inorg. Chem. Front.*, 2016, **3**, 1464–1472.
9 G. Audran, E. G. Bagryanskaya, I. Y. Bagryanskaya, M. Edeleva, P. Kaletina, S. R. Marque, D. Parkhomenko, E. V. Tretyakov and S. I. Zhivetyeva, *Inorg. Chem. Commun.*, 2018, **91**, 5–7.
10 N. Popova, G. Sysoeva, V. Nikolin, V. Kaledin, E. Tretyakov, M. Edeeva, S. Balakhnin, E. Lushnikova, G. Audran and S. Mark, *Bull. Exp. Biol. Med.*, 2017, **164**, 49–53.
11 D. Moncelet, P. Voisin, N. Koonjoo, V. r. Bouchaud, P. Massot, E. Parzy, G. r. Audran, J.-M. Franconi, E. Thiaudière and S. R. Marque, *Mol. Pharmaceutics*, 2014, **11**, 2412–2419.
12 G. Audran, E. Bagryanskaya, M. Edeleva, S. R. Marque, D. Parkhomenko, E. Tretyakov and S. Zhivetyeva, *Aust. J. Chem.*, 2018, **71**, 334–340.
13 M. V. Edeleva, S. R. Marque and E. G. e. Bagryanskaya, *Russ. Chem. Rev.*, 2018, **87**, 328.
14 G. Audran, R. Bikanga, P. Brémond, M. Edeleva, J.-P. Joly, S. R. Marque, P. Nkolo and V. Roubaud, *Org. Biomol. Chem.*, 2017, **15**, 8425–8439.
15 P. Nkolo, *Synthèse et étude physico-chimique de nouvelles alcoxyamines activables pour la lutte contre le paludisme*, Aix-Marseille University, 2017.
16 J. P. Blinco, S. E. Bottle, K. E. Fairfull-Smith, E. Simpson and K. Thomas, in *Nitroxide Mediated Polymerization; From Fundamentals to Applications in Materials Science*, ed. D. Gigmes, 2015, pp. 114–152.
17 S. R. Marque, in preparation.
18 D. Gigmes and S. R. A. Marque, in *Encyclopedia of Radicals in Chemistry, Biology and Materials*, ed. C. Chatgilialoglu and A. Studer, 2012, DOI: 10.1002/9781119953678.rad059.
19 E. G. Bagryanskaya and S. R. A. Marque, in *Nitroxide Mediated Polymerization: From Fundamentals to Applications in Materials Science*, ed. D. Gigmes, The Royal Society of Chemistry, 2016, pp. 45–113, DOI: 10.1039/9781782622635-00045.
20 D. Bertin, D. Gigmes, S. R. Marque and P. Tordo, *Macromolecules*, 2005, **38**, 2638–2650.
21 D. Bertin, D. Gigmes, S. R. Marque, S. Milardo, J. Peri and P. Tordo, *Collect. Czech. Chem. Commun.*, 2004, **69**, 2223–2238.
22 S. Marque, J. Sobek, H. Fischer, A. Kramer, P. Nesvadba and W. Wunderlich, *Macromolecules*, 2003, **36**, 3440–3442.
23 S. Marque, *J. Org. Chem.*, 2003, **68**, 7582–7590.
24 H. Fischer, A. Kramer, S. R. Marque and P. Nesvadba, *Macromolecules*, 2005, **38**, 9974–9984.
25 E. G. Bagryanskaya and S. R. Marque, *Chem. Rev.*, 2014, **114**, 5011–5056.
26 C. Y. Lin, S. R. Marque, K. Matyjaszewski and M. L. Coote, *Macromolecules*, 2011, **44**, 7568–7583.
27 J. L. Hodgson, C. Yeh Lin, M. L. Coote, S. R. Marque and K. Matyjaszewski, *Macromolecules*, 2010, **43**, 3728–3743.
28 C. Hansch, A. Leo and R. Taft, *Chem. Rev.*, 1991, **91**, 165–195.
29 P. Brémond, A. Koïta, S. R. Marque, V. Pesce, V. Roubaud and D. Siri, *Org. Lett.*, 2011, **14**, 358–361.
30 G. r. Audran, L. Bosco, P. Brémond, S. R. Marque, V. r. Roubaud and D. Siri, *J. Org. Chem.*, 2013, **78**, 9914–9920.
31 G. Audran, P. Brémond, M. B. B. Ibanou, S. R. Marque, V. Roubaud and D. Siri, *Org. Biomol. Chem.*, 2013, **11**, 7738–7750.
32 P. Nkolo, G. Audran, R. Bikanga, P. Brémond, S. R. Marque and V. Roubaud, *Org. Biomol. Chem.*, 2017, **15**, 6167–6176.
33 G. r. Audran, P. Brémond, S. R. Marque and G. Obame, *J. Org. Chem.*, 2013, **78**, 7754–7757.
34 A. Caneschi, D. Gatteschi, R. Sessoli, C. I. Cabello, P. Rey, A. L. Barra and L. C. Brunel, *Inorg. Chem.*, 1991, **30**, 1882–1886.
35 G. Sheldrick, *SHELX97 Programs for Crystal Structure Analysis (Release 97-2)*, University of Göttingen, 1997.
36 *Saint and SADABS, v. 2008-1*, Bruker AXS Inc., Madison, WI, USA, 2008.
37 A. Spek, *PLATON, a multipurpose crystallographic tool (Version 10M)*, Utrecht University, Utrecht, The Netherlands, 2003.
38 A. Spek, *J. Appl. Crystallogr.*, 2003, **36**, 7–13.
39 C. F. Macrae, P. R. Edgington, P. McCabe, E. Pidcock, G. P. Shields, R. Taylor, M. Towler and J. v. d. Streek, *J. Appl. Crystallogr.*, 2006, **39**, 453–457.